Multiphoton Photochemistry of Red Fluorescent Proteins in Solution and Live Cells

ARTICLE *in* THE JOURNAL OF PHYSICAL CHEMISTRY B · JULY 2014

Impact Factor: 3.3 · DOI: 10.1021/jp502477c · Source: PubMed

9 AUTHORS, INCLUDING:

Jack R Collins
National Institutes of Health
83 PUBLICATIONS **1,874** CITATIONS
SEE PROFILE

Geoffrey R Wicks
Newport-ILX Lightwave, Bozeman, MT
24 PUBLICATIONS **73** CITATIONS
SEE PROFILE

Thomas Hughes
Montana State University
89 PUBLICATIONS **3,274** CITATIONS
SEE PROFILE

Aleksander Rebane
Montana State University
239 PUBLICATIONS **4,531** CITATIONS
SEE PROFILE

THE JOURNAL OF PHYSICAL CHEMISTRY B

Article

pubs.acs.org/JPCB

Multiphoton Photochemistry of Red Fluorescent Proteins in Solution and Live Cells

Mikhail Drobizhev,*[,†] Caleb Stoltzfus,[†] Igor Topol,[§] Jack Collins,[§] Geoffrey Wicks,[†] Alexander Mikhaylov,[†] Lauren Barnett,[‡] Thomas E. Hughes,[‡] and Aleksander Rebane[†]

[†]Department of Physics and [‡]Department of Cell Biology and Neuroscience, Montana State University, Bozeman, Montana 59717, United States

[§]Leidos Biomedical Research, Inc., Frederick National Laboratory for Cancer Research, Frederick, Maryland 21702-1201, United States

Supporting Information

ABSTRACT: Genetically encoded fluorescent proteins (FPs), and biosensors based on them, provide new insights into how living cells and tissues function. Ultimately, the goal of the bioimaging community is to use these probes deep in tissues and even in entire organisms, and this will require two-photon laser scanning microscopy (TPLSM), with its greater tissue penetration, lower autofluorescence background, and minimum photodamage in the out-of-focus volume. However, the extremely high instantaneous light intensities of femtosecond pulses in the focal volume dramatically increase the probability of further stepwise resonant photon absorption, leading to highly excited, ionizable and reactive states, often resulting in fast bleaching of fluorescent proteins in TPLSM. Here, we show that the femtosecond multiphoton excitation of red FPs (DsRed2 and mFruits), both in solution and live cells, results in a chain of consecutive, partially reversible reactions, with individual rates driven by a high-order (3−5 photon) absorption. The first step of this process corresponds to a three- (DsRed2) or four-photon (mFruits) induced fast isomerization of the chromophore, yielding intermediate fluorescent forms, which then subsequently transform into nonfluorescent products. Our experimental data and model calculations are consistent with a mechanism in which ultrafast electron transfer from the chromophore to a neighboring positively charged amino acid residue triggers the first step of multiphoton chromophore transformations in DsRed2 and mFruits, consisting of decarboxylation of a nearby deprotonated glutamic acid residue.

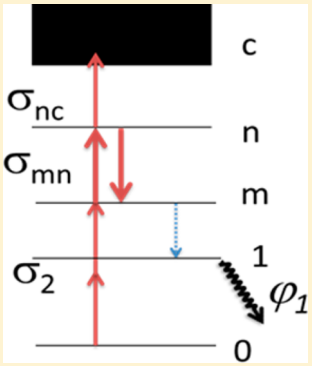

1. INTRODUCTION

Genetically encoded fluorescent proteins (FPs)[1] and biosensors make it possible to optically record cell signaling, migration, and death in living organisms, see, e.g., refs 2−4. Today, the most significant constraint to imaging deep inside whole organisms is the strong scattering and absorption of visible light by most of the tissues. Compared to wide-field and confocal microscopy, two-photon laser scanning microscopy (TPLSM)[5,6] provides a deep-penetrating, high-resolution, low-background, and low-damage solution for thick tissue imaging. Although TPLSM is becoming the method of choice for interrogation of tissues, fast multiphoton bleaching (MPB) inside the focal volume can be a serious limitation.[6] Here, we use the term multiphoton bleaching for the complex chain of reactions that leads to irreversible loss of original fluorescence upon laser excitation at a particular wavelength. If one fluorescent form is transformed to another in an individual step of the chain, then this process is called, herein, multiphoton transformation (MPT). Although these processes are generally disadvantageous, they can potentially be made advantageous for increasing the imaging depth and/or contrast. This can be accomplished by focal multiphoton activating/switching (or deactivating/bleaching) of an FP with one wavelength and then detecting its two-photon excited fluorescence (or its absence) with another wavelength.[7,8] In this case, the total fluorescence signal of the photoactivated subset of molecules depends on the laser intensity P stronger than quadratically (i.e., $F \sim P^{\beta}$, $\beta > 2$) because the photoactivation (or bleaching) reaction rate itself depends on the laser power nonlinearly. Therefore the fundamental limit of penetration depth for the classical two-photon imaging[9] can be broken, and deeper imaging can be attained.[7,8]

Red fluorescent proteins (RFPs), such as DsRed and its monomeric derivatives, are attractive for deep imaging because of their red-shifted fluorescence, but they bleach quickly compared to EGFP under typical TPLSM conditions, see Figure 1 and refs 4 and 10. Empirically, it has been demonstrated that the multiphoton photobleaching rate k of dyes and FPs (including RFPs) increases much more steeply with the increasing laser intensity than the expected quadratic law, i.e., as $k \sim P^{\alpha}$ with the exponent $\alpha = 2.5-5.3$.[11−16] It has been also observed that the bleaching rate of DsRed can be significantly reduced by tuning the laser wavelength from 720−760 to 950−1100 nm.[10,13] The MPB rate can also depend on

Received: March 11, 2014
Revised: July 2, 2014
Published: July 8, 2014

   dx.doi.org/10.1021/jp502477c | J. Phys. Chem. B 2014, 118, 9167−9179

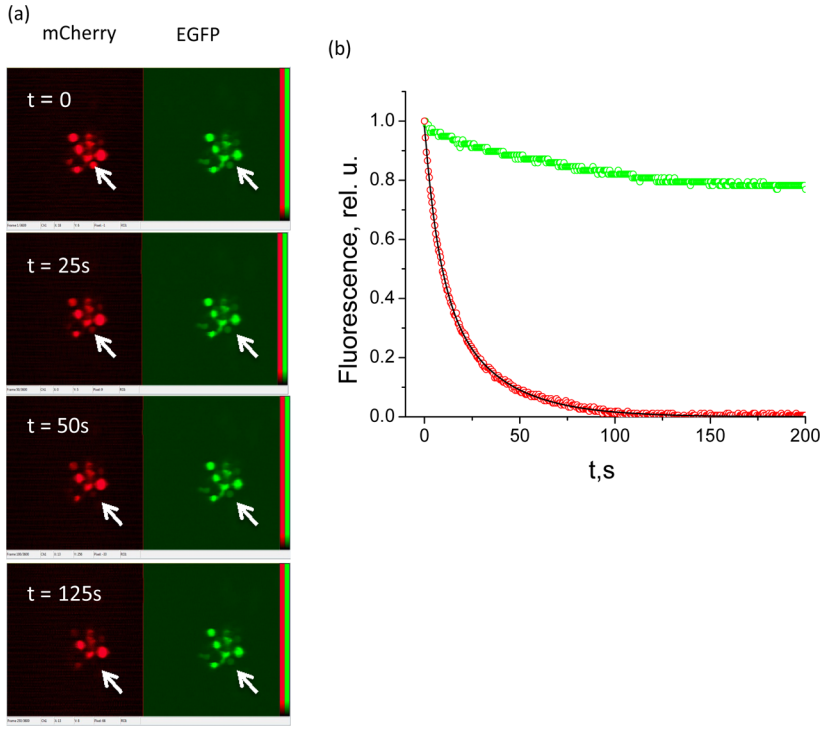

Figure 1. (a) TPLSM imaging of HEK cells cotransfected with EGFP (green) and mCherry (red). The frames from top to bottom correspond to 0, 25, 50, and 125 s of raster scanning, with the rate of 2 frames/s. (b) Temporal decay of the fluorescence signal of EGFP (green) and mCherry (red). The biexponential fit to the latter is shown by a continuous black line.

the biological environment, pulse duration, repetition rate, and so forth.[17−19] Although MPB has been observed by several groups, the underlying photophysics, particularly in RFPs, is not understood. A faster-than-quadratic power dependence of the photobleaching rate suggests an involvement of more than two photons in the process, but fundamental questions remain unanswered: Is the process instantaneous (three-, four-, or even more photon absorption) or stepwise, i.e., a sequential absorption of photon(s) after an initial simultaneous two-photon transition? If the process is stepwise, then does it involve a climbing upon higher singlet or triplet states? If it is a singlet−singlet excitation, then is there any energetic relaxation involved between the two-photon absorption (2PA) event and the additional photon(s) absorption? Why is the power exponent of the intensity dependence often a noninteger number? Is this because of a competition between different-order processes (e.g., two- and three-photon absorption) or because of saturation of one of the transitions?

The photochemical mechanisms are also not fully clarified. Recently, Habuchi et al. showed that upon consecutive absorption of two 532 nm photons by DsRed protein its chromophore first photoconverts to a much dimmer form (the so-called super red form) with red-shifted absorption (574 nm) and fluorescence (595 nm).[20] Absorption, fluorescence, and vibrational spectroscopy, as well as mass spectrometry, demonstrate that this transformation corresponds to the *cis*-to-*trans* isomerization of the chromophore coupled with the Kolbe decarboxylation of the nearby glutamate residue, most probably E215. Further irradiation results in bleaching of the super red form and in the appearance of the blue form, absorbing at ∼380 nm, which was tentatively assigned to a protonated state of the chromophore.[20] The Kolbe mechanism of GFP decarboxylation studied earlier[21] assumed electron transfer from the deprotonated E215 residue (we use the DsRed sequence numbering here and throughout) to the electronically excited (neutral) chromophore, with subsequent decarboxylation of E215 followed by back transfer of an electron plus proton (or whole hydrogen atom) from the chromophore to the $-CH_2^{\bullet}$ radical of the transient E215 residue. In the case of DsRed, it is unclear, however, if the anionic chromophore, even in the electronically excited state, would have enough electron affinity to accept the second electron (see ref 22), and, because the chromophore is initially deprotonated, the particular chemical group in the protein that would serve as the electron and proton (or hydrogen atom) donor for the E215 residue is not established. Further uncertainty to the sequence of events of the MPT process is added by the fact that the electron detachment energy of the DsRed chromophore in vacuum is quite low, ∼3.27 eV[23] (which corresponds to a 380 nm one-photon excitation or a 760 nm two-photon excitation). Therefore, it is not clear if the first step of multiphoton-induced transformation would be electron detachment or acceptance, which is followed by the Kolbe reaction in the latter case.

Here, we study MPT and MPB of four mutants of DsRed: a faster-maturing mutant DsRed2,[24] whose optical properties are virtually identical to DsRed, and the monomeric mFruit variants mCherry,[25] mStrawberry,[25] and mPlum.[26] The MPB kinetics measurements were performed in three different experimental settings. First, we used typical TPLSM conditions (NA = 0.8) and scanning mode for the MPB measurement in human embryonic kidney (HEK) cells coexpressing mCherry and EGFP to qualitatively compare their relative bleaching rates. In the second setup, we used purified proteins in buffer solution and low-repetition rate (1 kHz) excitation with a Ti:Sa amplifier to quantitatively characterize the bleaching dynamics and rates of RFPs. In the third setup, we studied the power dependences of the photobleaching rates in live *E. coli* colonies

dx.doi.org/10.1021/jp502477c | J. Phys. Chem. B 2014, 118, 9167−9179

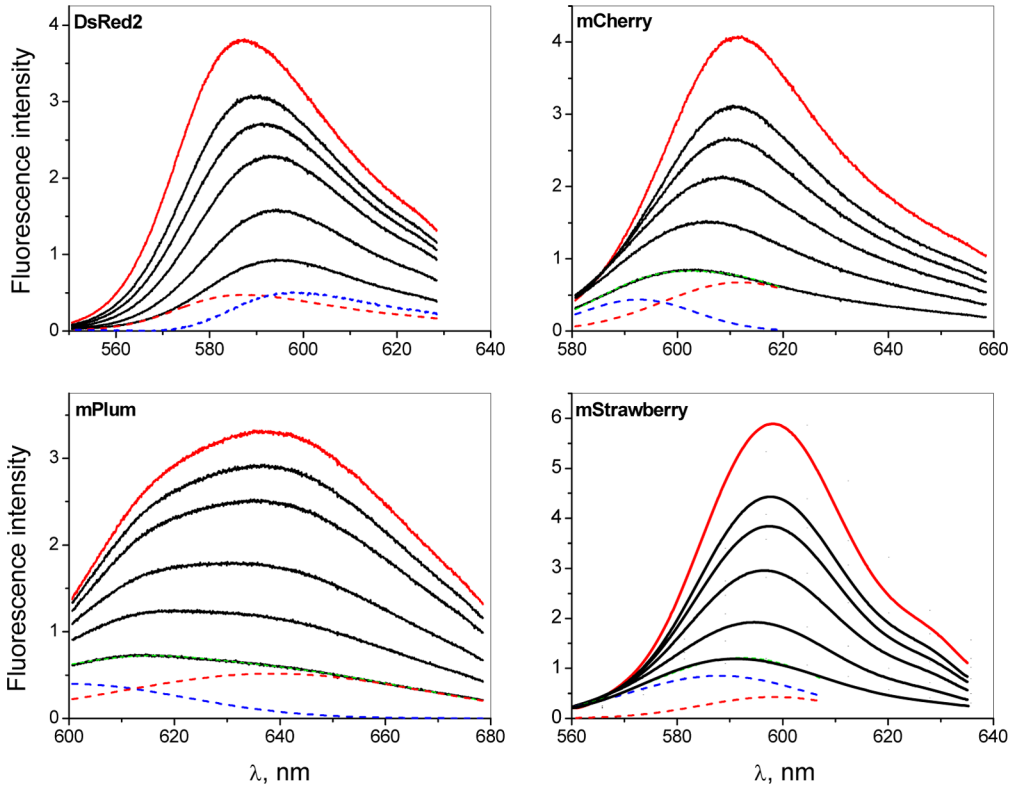

Figure 2. Fluorescence spectral changes during multiphoton irradiation of RFPs. The average power density is $P = 11.4$ W/cm^2. The top spectrum corresponds to irradiation time $t = 0$, and the bottom spectrum corresponds to the maximum total irradiation time of 3039 s for DsRed2, 1667 s for mCherry, 611 s for mPlum, and 3583 s for mStrawberry. Intermediate spectra, from top to bottom, correspond to several intermediate time points. Dashed lines show spectral contributions from the initial (red) and intermediate (blue) forms at the late stage of bleaching.

using the TPLSM setup (76 MHz repetition rate) in order to compare the bleaching rates under high- and low-repetition rate conditions as well as to investigate the role of the local surrounding (buffer vs cell). To keep the other experimental conditions the same, we used the 790 nm excitation wavelength in all three setups because this is the working (fixed) wavelength of the Ti:Sa amplifier. Using the experimental data, multiphoton excitation kinetics models, and quantum calculations of the energetics of elementary reactions, we were able to clarify the photophysical mechanism of the first step of the MPB process and propose the mechanisms of the next consecutive steps in RFP phototransformation and bleaching.

2. RESULTS

2.1. Fast Multiphoton Bleaching of mCherry upon TPLSM Imaging of HEK Cells Coexpressing mCherry and EGFP. Figure 1a shows the consecutive images of a group of HEK cells coexpressing mCherry and EGFP under typical TPLSM conditions (see Supporting Information for technical details).

The fluorescence signal was collected simultaneously in the green and red channels. One selected cell, marked by an arrow, likely received the most power because of the optimum z-position and, as a result, completely lost its red (mCherry) fluorescence after ∼100 s. On the other hand, the EGFP fluorescence of the same cell decreased by only ∼20%. The temporal dependence of the fluorescence in the red and green channels, both normalized to 1 at $t = 0$, is shown in Figure 1b. This experiment demonstrates that mCherry bleaches much faster than EGFP under the same experimental conditions. It is interesting to note that the fluorescence decay of mCherry can be well-described by a sum of two exponents with zero offset (see the full line in Figure 1b). The nature of this biexponential behavior is studied in the next section.

2.2. Multiphoton Bleaching of Purified Proteins in Solution. *2.2.1. Unraveling Kinetic Schemes.* In these experiments, we irradiate buffered solutions of RFPs with the Ti:Sa amplifier laser system operated at 790 nm wavelength, 1 kHz repetition rate, and 120 fs pulse duration, with a uniform distribution of the power density across the sample (see the Supporting Information for more details). We monitor the concentrations of the initial and intermediate forms by recording time-dependent fluorescence spectra during MPB. Figure 2 shows the series of selected fluorescence spectra of DsRed2 and mFruits during the irradiation process. Because the same laser is used for both irradiation and interrogation, these 2PEF spectra reflect the time-dependent evolution of the concentration of initial, as well as photoconverted, fluorescent species, which can be excited by the 790 nm pulses.

As can be seen, the decrease in the total intensity is accompanied by a shift of the peak position to the blue in mFruits and to the red in DsRed2. Qualitatively similar behavior was previously observed for mPlum[27] and DsRed.[20] Spectral deconvolution with a few Gaussians, having the same central frequencies and widths but different amplitudes for different time points, shows that all of the spectra at every time point can be well-described by two main contributions: the initial (unbleached) form and a new, spectrally shifted intermediate form. The peak position of the intermediate form varies much less within the series than that of the initial form: from 588 nm in mStrawberry to 593 nm in mCherry, 596 nm in DsRed2, and 600 nm in mPlum. This new band,

dx.doi.org/10.1021/jp502477c | J. Phys. Chem. B 2014, 118, 9167−9179

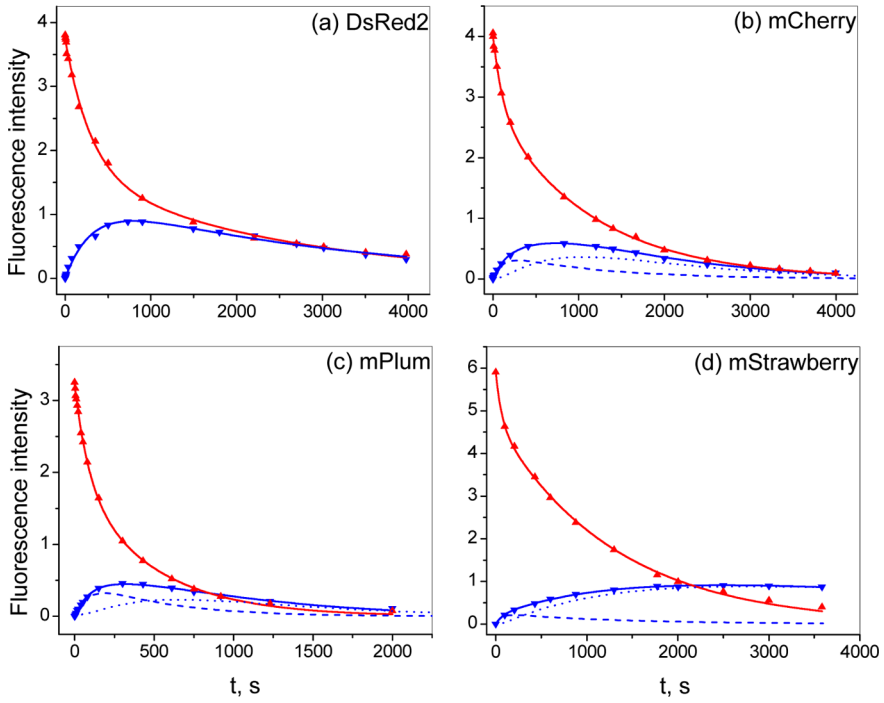

Figure 3. Decay kinetics of the initial (red symbols) and intermediate (blue symbols) forms. The solid continuous lines show the corresponding fitting functions (see the text for details). The dashed blue line represents the contribution of structure *B* and the dotted blue line represents the contribution of structure *C* to the fluorescence of intermediate form in the case of the mFruits (see the text for details).

Table 1. Multiphoton Bleaching Rates upon Irradiation of the Buffer FP Solutions with a Ti:Sa Amplifier[a]

protein	k_1, s^{-1}	k_1*, s^{-1}	k_2, s^{-1}	k_3, s^{-1}	k_4, s^{-1}
DsRed2	1.4×10^{-3}	1.4×10^{-3}	9.8×10^{-4}	6.5×10^{-4}	
mCherry	2.8×10^{-3}	2.4×10^{-3}	6.7×10^{-3}	2.6×10^{-3}	1.4×10^{-3}
mPlum	3.5×10^{-3}	3.2×10^{-3}	3.4×10^{-3}	4.0×10^{-3}	1.5×10^{-3}
mStrawberry	1.5×10^{-3}	1.1×10^{-3}	9.2×10^{-3}	3.3×10^{-3}	1.4×10^{-4}

[a]The rates of the individual steps of the kinetics eq 1 for DsRed2 and eq 5 for mFruits. k_1* is the rate of the first step, calculated according to the cross-sections and quantum yields obtained in the experiment with the repetition rate f = 76 MHz in *E. coli* bacteria but with laser parameters corresponding to the amplifier experiment (*vide infra*). Experimental errors of the k values are ~20%.

appearing in the DsRed spectrum at 596 nm, was previously assigned to the *trans* anionic form of the chromophore (super red form).[20] Similarly, the fluorescence peak near 611 nm was shown to correspond to the *trans* anionic form of two other red FPs, possessing the same chromophore structure as DsRed, i.e., eqFP611 and d2RFP630.[28] The photoproducts with the same fluorescence spectra, peaking between 590 and 600 nm, can also be created by one-photon irradiation of mFruits (Supporting Information Figure 8) and were also previously assigned to the *trans* isomers.[29−31] On the basis of these observations, we attribute the peak near 590−600 nm (Figure 2) to the anionic *trans* isomer of the DsRed-like chromophore in all RFPs studied here.

Figure 3 shows the temporal changes of the amplitudes of the initial (red symbols) and intermediate (blue symbols) forms. The kinetics of the initial form can be well-described by a biexponential decay with zero offset for all four proteins. This suggests at least a two-step consecutive reaction with a reversible first step.

DsRed2. In the case of DsRed2, the simplest reaction scheme that consistently describes the kinetics of both the initial and intermediate states is presented by eq 1

$$A \underset{k_2}{\overset{k_1}{\rightleftarrows}} B \overset{k_3}{\rightarrow} C \tag{1}$$

Where A, B, and C are the concentrations of the initial, intermediate, and final forms, respectively; k_1, k_2, and k_3 are the corresponding rate constants. The solution of the corresponding system of differential equations (shown only for A and B here) reads

$$A = \frac{A_0}{\gamma_1 - \gamma_2}[(\gamma_1 - k_2 - k_3)e^{-\gamma_1 t} + (k_2 + k_3 - \gamma_2)e^{-\gamma_2 t}],$$

$$\text{where } A_0 = A(0) \tag{2}$$

$$B = \frac{A_0 k_1}{\gamma_1 - \gamma_2}[e^{-\gamma_2 t} - e^{-\gamma_1 t}] \tag{3}$$

where

$$\gamma_1\gamma_2 = k_1k_3; \quad \gamma_1 + \gamma_2 = k_1 + k_2 + k_3 \tag{4}$$

Because the fluorescence signal F is proportional to the concentration of the corresponding form, we use functions 2 and 3 to describe the experimental decay kinetics up to a constant factor. We first obtained the rates k_1 from the initial slope of the normalized (as $F(0) = 1$) decay curves (method of

dx.doi.org/10.1021/jp502477c | J. Phys. Chem. B 2014, 118, 9167−9179

initial rates). We then fitted the experimental decay of the initial (A) form to a biexponential decay $F = a\exp(-\gamma_1 t) + b\exp(-\gamma_2 t)$ (red line in Figure 3a) and obtained $\gamma_1 = (3.2 \pm 0.4) \times 10^{-3}$ s^{-1} and $\gamma_2 = (4.0 \pm 0.4) \times 10^{-4}$ s^{-1}. Using k_1 and solving eq 4, we found k_2 and k_3. All of the rates are presented in Table 1 (second row).

Independent fitting of the kinetics of the intermediate (B) form to the function $F = c[\exp(-\gamma_2 t) - \exp(-\gamma_1 t)]$, shown by a blue line in Figure 3, results in $\gamma_1 = (3.2 \pm 0.3) \times 10^{-3}$ s^{-1} and $\gamma_2 = (3.4 \pm 0.3) \times 10^{-4}$ s^{-1}. Both values coincide, within experimental error margins, with the corresponding values found from the decay of form A. This justifies eq 1 for DsRed2, where state B can be attributed to the anionic *trans* chromophore of the super red form. State C probably corresponds to a protonated form of the chromophore, absorbing near 380 nm and nonfluorescent in the 560−630 nm window.[20,32] A similar scheme, but without the back reaction ($k_2 = 0$), was used to quantitatively describe the DsRed kinetics in ref 20. These authors used two-photon stepwise (1 + 1) excitation with 532 nm nanosecond pulses. The difference in the kinetic schemes used here and those in ref 20 probably arises from the fact that the reverse $B \rightarrow A$ reaction in our case is also activated by multiphoton stepwise absorption, which requires high instantaneous peak power of femtosecond pulses. This is further supported by the observation of biexponential decay (i.e., with reverse reaction) in DsRed2 upon femtosecond excitation in TPLSM setup, see Figure 1 and ref 10.

Note that the reaction scheme $B \leftrightarrow A \rightarrow C$, where A, B, and C are the initial, intermediate, and final forms, respectively, can describe the observed kinetics as well. According to ref 20, however, the $B \rightarrow C$ step is non-negligible, which makes us inclined to the scheme in eq 1.

mFruits. We first found that eq 1 could not consistently (i.e., with the same parameters, k_1, k_2, and k_3) explain the kinetics of both the A and B forms in mFruits. The minimum scheme that satisfactorily described the decays needed an additional step $C \rightarrow D$ and is given in eq 5

$$A \underset{k_2}{\overset{k_1}{\rightleftarrows}} B \overset{k_3}{\rightarrow} C \overset{k_4}{\rightarrow} D \tag{5}$$

where B and C are some intermediate forms and D is a final form. The solution of the underlying differential equations (shown only for A, B, and C) reads

$$A = \frac{A_0}{\gamma_1 - \gamma_2}[(\gamma_1 - k_2 - k_3)e^{-\gamma_1 t} + (k_2 + k_3 - \gamma_2)e^{-\gamma_2 t}],$$
$$\text{where } A_0 = A(0) \tag{6}$$

$$B = \frac{A_0 k_1}{\gamma_1 - \gamma_2}[e^{-\gamma_2 t} - e^{-\gamma_1 t}] \tag{7}$$

$$C = A_0 k_1 k_3\left[\frac{e^{-k_4 t}}{(\gamma_1 - k_4)(\gamma_2 - k_4)} + \frac{e^{-\gamma_1 t}}{(\gamma_1 - \gamma_2)(\gamma_1 - k_4)} + \frac{e^{-\gamma_2 t}}{(\gamma_1 - \gamma_2)(k_4 - \gamma_2)}\right] \tag{8}$$

where

$$\gamma_1\gamma_2 = k_1k_3; \quad \gamma_1 + \gamma_2 = k_1 + k_2 + k_3 \tag{9}$$

Interestingly, we also found that neither eq 7 nor 8 can separately describe the kinetics of the intermediate form (blue symbols in Figure 3b−d), but their linear combination can. To obtain the rate constants, we first fitted the experimental decay of the initial form to a biexponential decay of the form $F = a\exp(-\gamma_1 t) + b\exp(-\gamma_2 t)$, cf. eq 6 (red line in Figure 3b−d), and found γ_1 and γ_2. We then fitted the kinetics of the intermediate form to the following function (i.e., linear combination of eqs 7 and 8)

$$F = \nu\left[\frac{1}{(\gamma_1 - k_4)(\gamma_2 - k_4)}e^{-k_4 t} + \left(\frac{1}{(\gamma_1 - \gamma_2)(\gamma_1 - k_4)} - \frac{\mu}{\nu}\right)e^{-\gamma_1 t} + \left(\frac{1}{(\gamma_1 - \gamma_2)(k_4 - \gamma_2)} + \frac{\mu}{\nu}\right)e^{-\gamma_2 t}\right] \tag{10}$$

where the γ_1 and γ_2 values were fixed and equal to those found above, and three other parameters, μ, ν, and k_4, were free. Here, the factors μ and ν represent the relative contributions of forms B and C to the total fluorescence signal, respectively. The fitting curves are shown by blue lines in Figure 3b−d and, as one can see, describe the data quite well. Again, using the independently obtained k_1 values from the initial slope, we found k_2 and k_3 from eq 9. All of these rates are presented in Table 1, lines 3−5. Knowing μ and ν, we show individual contributions from the B (dashed line) and C (dotted line) forms in Figure 3b−d.

At first glance, it is quite surprising that the fluorescence spectrum of the intermediate form (590−600 nm), consisting of only one isolated and narrow peak (Supporting Information Figure 9), contains contributions from two chemically different forms (i.e., B and C) appearing at the different stages of bleaching. One reasonable explanation is that the B and C forms correspond, respectively, to the *trans*-chromophore with deprotonated and protonated (in the ground state) phenoxy group, which have different absorption but identical fluorescence spectra. If the protonated form undergoes fast excited-state proton transfer, similar to what has recently been described for other RFPs, including mKeima,[33] LSSmKate, and LSSmCherry,[34] then its fluorescence spectrum will match perfectly with that of the initially deprotonated form. This assumption is further supported by the appearance of a characteristic absorption peak near 465 nm at the late stages of bleaching (Supporting Information Figure 10), which has been assigned to a protonated DsRed-like chromophore in a *trans*-conformation.[34] The ratio of deprotonated to protonated (absorbing at 575 nm) forms in the absorption spectrum indicates that the anionic form appears first (B) and then transforms to the neutral one (C). Because both forms have overlapping 2PA spectra with similar cross-sections at 790 nm (cf. 2PA spectrum of, e.g., TagRFP[35] with that of LSS-mKate2[36]), they contribute similarly to the fluorescence signal at an intermediate bleaching stage ($t \sim 1000$ s) (Figure 3b−d). Therefore, in contrast to DsRed, mFruits undergo an additional photoconversion step, i.e., from an anionic to a neutral form in the process of MPB. The D form can be similar in nature as that of the C form in DsRed2 (see above).

2.2.2. Power Dependence of the Rates of Individual MPT Steps in mPlum. To gain further insight into the mechanisms of MPB, we studied the dependence of individual MPT rates, involved in eq 5, as a function of laser power. For these experiments, we selected mPlum because it bleaches quickly

dx.doi.org/10.1021/jp502477c | J. Phys. Chem. B 2014, 118, 9167−9179

even at low power. The fluorescence signal was collected in the region of 630−680 nm, i.e., where the fluorescence of forms *B* and *C* is negligible (Figure 2). We first checked that the initial (unbleached) fluorescence depended quadratically on power (Supporting Information Figure 11), implying that the simultaneous 2PA transition is not saturated. Using the method of initial rates (see above), we obtained k_1 as a function of power over a broad power range. Figure 4a shows the

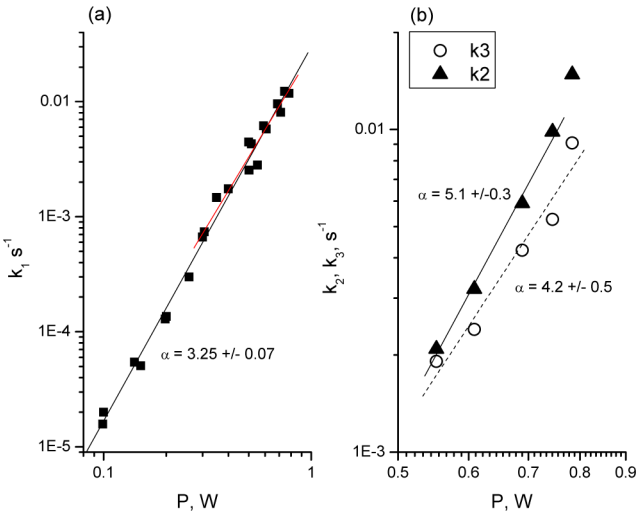

Figure 4. Power dependence of the (a) first step rate k_1 and (b) reverse step rate k_2 and second step rate k_3 for mPlum in solution upon irradiation with a Ti:Sa amplifier.

dependence of k_1 on the average power P in a double-logarithmic scale. Describing the dependence with an empirical power law

$$k_1 \sim P^{\alpha} \tag{11}$$

we find α = 3.25, which means that a four-photon process is involved in the $A \rightarrow B$ transformation. The noninteger value of α suggests that either four photons, in total, are absorbed, but some of the transitions are saturated, or that the four-photon process competes with lower-order (two- or three-photon) processes.

The power dependences of the next consecutive steps of eq 5 were measured in a high-power region (0.55−0.8 W), where it was possible to obtain enough dynamic range of the decay in a reasonable amount of time. The decay curves were fitted with a biexponential function, and rates k_2 and k_3 were obtained as described in the previous section. The power dependences of k_2 and k_3 are shown in Figure 4b. Because $k_2 \sim P^5$, the back (*trans*−*cis*) reaction is photoactivated and requires at least five photons. The next, $B \rightarrow C$, reaction (leading to chromophore protonation) is also multiphoton-induced and consumes at least four photons.

2.2.3. Dependence of k_1 on Pulse Duration for DsRed2 and mPlum. Our next step was to discriminate between the simultaneous (coherent) *n*-photon absorption ($n > 2$) and stepwise 2 + 1 or 2 + 1+1 processes, where the simultaneous two-photon absorption is followed by the stepwise excited-state absorption of additional photons. To this end, we investigated the dependence of k_1 on the pulse duration. Becase, in a simultaneous process, the absorption rate depends on the instantaneous intensity within the pulse, one would expect a quadratic decrease of the bleaching rate with the increase of pulse duration for the simultaneous three-photon process and a cubic decrease for the simultaneous four-photon process. In contrast, the linear decrease is expected for the stepwise case. In our experiment, a 2-fold elongation of the pulse from 120 to 240 fs (while keeping the pulse energy unchanged) resulted in a 2-fold decrease of the initial decay rate for DsRed2 and mPlum (Supporting Information Figure 12), justifying the stepwise mechanisms. This result is not very surprising because the simultaneous multiphoton absorption processes usually dom-

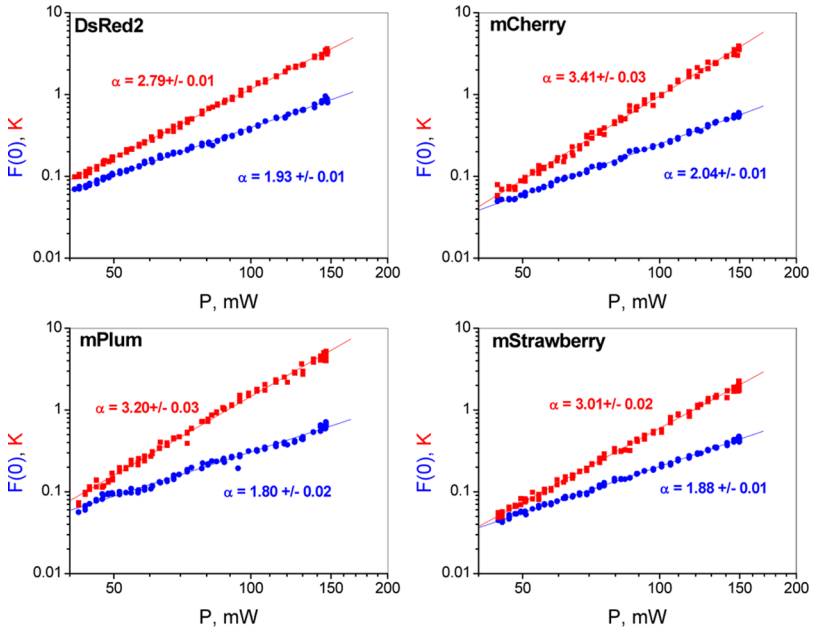

Figure 5. Dependence of the initial fluorescence signal $F(0)$ (blue symbols) and initial photobleaching rate K (red symbols) on average laser power plotted on a double-logarithmic scale. Both $F(0)$ and K were fitted with the empirical power law function P^{α}. The best fit values of α are depicted for each protein. Bleaching was monitored in live *E. coli* colonies.

dx.doi.org/10.1021/jp502477c | J. Phys. Chem. B 2014, 118, 9167−9179

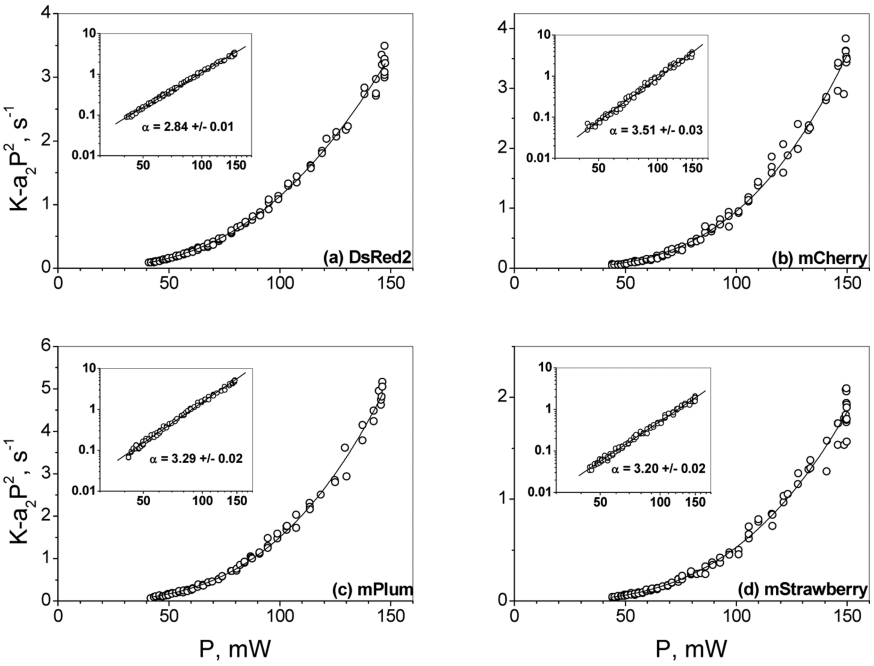

Figure 6. Power dependence of the initial rate of photobleaching less the two-photon induced contribution (a_2P^2). Symbols represent the experimental data, and continuous lines show fitting to eq 15 for DsRed2 and eq 18 for mFruits (see the text for explanations). The insets show the same plots on a double-logarithmic scale. The best linear fits (straight lines) and their corresponding slopes α are also shown.

inate only if the intermediate states are virtual. In the systems considered here, the excited states lying higher than the S_1 state make a quasi-continuum, thus always providing a real intermediate state for the third and fourth photon absorption. Given the stepwise mechanisms, we can make a further conclusion based on our result that the energetic (vibrational) relaxation between the sequential absorption events (in 2 + 1 or 2 + 1 + 1 processes) does not occur on the time scale of ~100−200 fs. Otherwise, the underlying molecular cross sections would change for different pulse durations, which would result in a change of the bleaching rate by a factor other than 2. Therefore, if there is any relaxation, then it should be either much faster than 100 fs or slower than 200 fs. The former would be quite unusual, even for the macromolecular systems studied here. The latter possibility will be studied in Section 2.4.5.

2.3. Multiphoton Bleaching of RFPs Expressed in Live *E. coli* Bacteria. In this set of experiments, we measured the fluorescence bleaching kinetics $F(t)$ in live *E. coli* bacteria using the two-photon microscope setup with a high repetition rate (76 MHz) (see the Supporting Information). Because of the strong nonuniformity of the laser intensity across the focal volume and the non-mono-exponential character of the intrinsic bleaching kinetics (see above), the observed decay curves could not be described with a sum of a reasonable number of exponents (Supporting Information Figure 13). Therefore, here, we use the method of initial rates to measure an effective rate K of the first, $A \rightarrow B$, step as a function of laser power. The thus obtained value of K is a result of averaging of the local initial rates k_1 over space across the focal volume. Figure 5 shows the dependence of both K and the initial fluorescence signal, $F(0)$, on power for DsRed2 and mFruits. Although $F(0)$ increases nearly quadratically, the photobleaching rate shows a much steeper dependence on power. The power exponent of eq 11 varies from $\alpha = 2.79$ to 3.41. The value obtained for mPlum ($\alpha = 3.20$) is close to what was measured at 1 kHz excitation (cf. Figure 4a), suggesting that the order of the processes (number of photons involved) does not depend on the repetition rate or on the local protein environment (water vs cell). Because α is always larger than 2, we can conclude that the three- or four-photon excitation of higher excited states is responsible for multiphoton transformations.

2.4. Phenomenological Model of the First Step of MPB. *2.4.1. Why Is the Power Exponent α Noninteger?* The power exponent α of the intensity dependence of photobleaching rates (Figure 5) in most cases is a noninteger number. Physically, this can be explained either by a competition between parallel two-, three-, four-, and so on photon-induced processes[37] or by saturation of a certain transition in the multiphoton consecutive ladder process.[38,39] In the former case, the microscopic rate k_1 is described by a sum of the rates of processes with different photon orders[37]

$$k_1 = k_1^{(2)} + k_1^{(3)} + k_1^{(4)} + \ldots \quad (12)$$

After integration of the individual contributions in eq 12 over space and explicitly expressing power dependences of the corresponding process, we arrive at the polynomial function

$$K = K^{(2)} + K^{(3)} + K^{(4)} + \ldots = a_2P^2 + a_3P^3 + a_4P^4 + \ldots \quad (13)$$

where all of the coefficients a_n are positive. In the second case, if any of the consecutive transitions involved in an n-photon absorption process is saturated, then, as can be shown (Supporting Information), the corresponding rates $k_1^{(n)}$ and $K^{(n)}$ can be described by an analytical function, which can be approximated in the limiting cases of the slight or moderately strong saturation by a polynomial function of P, where some of the coefficients turn negative. Therefore, careful analysis of the experimental power dependence of the higher order (3−4 photons) MPT rate will allow one to distinguish between the

dx.doi.org/10.1021/jp502477c | J. Phys. Chem. B 2014, 118, 9167−9179

Table 2. Molecular Parameters Involved in Multiphoton Bleaching of RFPs[a]

protein	ESE, eV	VDE, eV	ADE, eV	σ_2[b] GM	σ_{mn}, cm^2	σ_{nc}, cm^2	φ_n	φ_1[c]
DsRed2	−3.97	7.24	7.12	10	3.0×10^{-17}		8.8×10^{-3}	7.1×10^{-5}
mCherry	−2.25	5.52	5.40	29	3.4×10^{-16}	1.81×10^{-19}		1.3×10^{-5}
mPlum	−2.34	5.61	5.49	43	8.7×10^{-16}	1.57×10^{-19}		3.8×10^{-6}
mStrawberry	−2.31	5.58	5.46	13	7.9×10^{-16}	1.85×10^{-19}		4.5×10^{-5}

[a]ESE is the calculated electrostatic interaction energy of the chromophore and surrounding protein; VDE is the vertical electron detachment energy in protein; ADE is the adiabatic electron detachment energy in protein; the definitions of the molecular parameters are the same as those in Figure 7. [b]Ref 35. [c]Ref 31.

two cases. In any of the above mechanisms, the photochemical reaction starting from the S_1 state that becomes populated after the initial 2PA step cannot be ruled out. We first calculate the contribution $K^{(2)}$ in the whole power range of Figure 5. By neglecting saturation of the 2PA transition ($F(0)$ depends quadratically on P), one can show (Supporting Information) that

$$K^{(2)} = a_2 P^2 = 0.076 \frac{\sigma_2 \phi_1}{f(h\nu)^2 \Delta\tau w_0^4} P^2 \quad (14)$$

where σ_2 is the two-photon cross-section at the excitation wavelength, φ_1 is the quantum yield of the reaction starting from the lowest excited state (S_1), f is the pulse repetition rate, h is Plank's constant, ν is the photon frequency, $\Delta\tau$ is the pulse duration, w_0 is the laser beam width at the focal plane, and P is the average power. According to Kasha's rule, φ_1 does not depend on the method of excitation (one- or two-photon). To evaluate a_2, we therefore can use the values of φ_1 previously determined in one-photon bleaching experiments,[31] as well as the known σ_2 values[35] and laser parameters. We then calculated the a_2P^2 contribution and subtracted it from the total rate K to obtain the power dependences of the higher order (three- or four-photon) processes. Although $K^{(2)}$ turns out to be several times smaller than K in the whole power range, this correction still provides more careful evaluations of $K^{(3)}$ and $K^{(4)}$ or of their combination. The results are shown in Figure 6, where the insets present the same plots on a double-logarithmic scale. For DsRed2, $\alpha = 2.84$, from which we conclude that, in total, three photons are involved in photobleaching and the third-photon absorption is slightly saturated. (The first, simultaneous 2PA transition is not saturated because the initial fluorescence depends quadratically on power.) For mFruits, the analysis shows that a combination of the nonsaturated third and fourth power terms in eq 13 cannot explain the observed power dependence (coefficient a_4 turns negative), and we conclude that four photons are involved and at least one of the subsequent excited-state transitions is moderately strongly saturated.

We thus arrive at a mechanism where the initial instantaneous 2PA is followed by an ultrafast (within ~100 fs) absorption of one additional photon in DsRed2 and two additional photons in mFruits. In all cases, at least one of the excited-state transitions is saturated to a certain extent. To specify the molecular mechanism of the first step, we estimate, in the next section, the number of photons required for the multiphoton detachment of an electron and discuss if this process might be responsible for the MPT in the proteins under investigation.

2.4.2. How Many Photons Are Needed to Photodetach the Electron? If there is enough total energy supplied to a HOMO electron of the chromophore, then the electron eventually will move away from the chromophore and from its local environment. Here, we estimate how many photons are required to accomplish this work. The total threshold photodetachment energy is DE = DE_0 − ESE, where DE_0 is the gas phase detachment energy from the chromophore, and ESE is the electrostatic interaction energy of the chromophore with the rest of the protein before the electron was detached. (We neglect the energies of the interaction of the neutral chromophore and of the quasi-free electron with their surroundings and with each other.) Ghosh et al. calculated the vertical detachment energy, VDE_0 = 3.27 eV, and adiabatic detachment energy, ADE_0 = 3.15 eV, for the model red chromophore in vacuum.[23] Our calculations of ESE (see the Supporting Information), employing the quantum-mechanical cluster approach for the first layer of the chromophore's surrounding[40] and the coarse grain point-charge simulation of the remaining protein, resulted in the values shown in Table 2. All of the ESE values are negative, meaning that the chromophore-bound electron is additionally stabilized by its protein surrounding. Interestingly, the potential well created by the surrounding is 1.7 V deeper in DsRed than in mFruits. This is due to one extra positive charge in the nearest chromophore environment, i.e., a combination of two positive and one negative charges: K83(+), K163(+), and E215(−) in DsRed compared to all three neutral corresponding positions in mFruits.[41,42] In the case of vertical photodetachment, i.e., without any energetic relaxation between instantaneous 2PA and additional photons absorption, the inequality $nh\nu$ > VDE must hold, where n is the total number of photons absorbed. Because $h\nu$ = 1.57 eV in our experiment, it is clear that for DsRed2 at least five photons are required to detach the electron (see Table 2). The experimentally observed power dependence ($\alpha \approx 2.8$) of the DsRed2 bleaching rate (Figure 6a) suggests that the MPT reaction does not involve electron photodetachment but rather proceeds through some other mechanism involving a bound highly excited state of the chromophore. In the case of mFruits, if the process of MPT would occur without relaxation, then four photons would suffice to overcome the photodetachment energy. However, if an energetic relaxation to the lowest vibrational level of the S_1 state occurred after an instantaneous absorption of two photons, then a total of five photons would be required to overcome the adiabatic barrier of detachment. Relaxation to a triplet state will lead to even larger energy losses and even more stringent requirements for the number of photons. Relating these data to the bleaching power dependence (Figure 6), we conclude that the reaction most probably proceeds through the vertical, i.e., without relaxation, four-photon electron detachment in mFruits, in agreement with the experimental dependence of the bleaching rate on pulse duration.

2.4.3. DsRed2: Parameters of the Three-Photon Photoconversion. The first step of the MPB process in DsRed2 can be presented by a three-level model shown in Figure 7a.

dx.doi.org/10.1021/jp502477c | J. Phys. Chem. B 2014, 118, 9167−9179

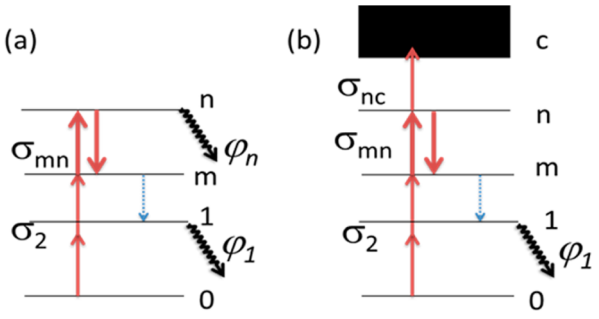

Figure 7. Energy level diagrams used to model the MPT process. The first step of MPB corresponds to a simultaneous 2PA, described by the cross section σ_2. After excitation of level m, the chromophore can relax nonradiatively (wavy blue arrow) to the lowest excited state 1 and then relax back to the ground state 0 or convert photochemically to a different structure with the quantum yield φ_1. Being excited to state m, the chromophore can be further promoted to a higher level, n, via excited-state transition with the one-photon cross section σ_{mn}. In DsRed2 (a), the photochemical reaction starting from level n is characterized by quantum efficiency φ_n. In mFruits (b), the additional, fourth, step is the transition from the excited state n into a level c belonging to the continuum of quasi-free states with the corresponding effective photodetachment cross section σ_{nc}.

The effective decay rate $K^{(3)}$ calculated with the possibility of slight saturation in the $m \rightarrow n$ transition (Supporting Information) reads

$$K^{(3)} = BP^2\left(0.132\frac{P}{P_s} - 0.033\left(\frac{P}{P_s}\right)^2\right) \tag{15}$$

where

$$B = \frac{\sigma_2\phi_n}{\pi^2 f(h\nu)^2\Delta\tau w_0^4} \tag{16}$$

and

$$P_s = \frac{\pi}{4}\frac{fh\nu w_0^2}{\sigma_{mn}} \tag{17}$$

is the saturation power. For definitions of the molecular parameters, see Figure 7. B and P_s were used as free parameters to fit experimental data to eq 15, see Figure 6a. Substituting the laser parameters and σ_2 (790 nm) = 10 GM (1GM = 10^{-50} cm^4 s),[35] we find σ_{mn} from the P_s value, using eq 17, and φ_n from the B value, using eq 16. The results are shown in Table 2.

2.4.4. mFruits: Parameters of the Four-Photon Phototransformation. For mFruits, we use the four-level model that, in addition to levels 0, m, and n, includes level c, belonging to a continuum (see Figure 7b). The resulting first step rate, when the $m \rightarrow n$ transition is close to saturation (but not fully saturated), reads (Supporting Information)

$$K^{(4)} = B'P\left(0.06642\left(\frac{P}{P_s}\right)^2 - 0.1855\frac{P}{P_s} + 0.2851\right) \tag{18}$$

where

$$B' = \frac{1}{4\pi}\frac{\sigma_{nc}\sigma_2}{\sigma_{mn}^2\Delta\tau h\nu w_0^2} \tag{19}$$

and P_s is given by eq 17. Figure 6b–d shows the fits of experimental data to eq 18. The fitting parameters P_s and B', in combination with laser parameters, allow us to obtain σ_{mn} and σ_{nc}, respectively (Table 2).

2.4.5. Are There Long-Lived States Involved in the First Step of MPB? Our next aim was to understand if the additional photons of the 2 + 1 and 2 + 1 + 1 processes are absorbed on the fast (i.e., singlet–singlet) or the longer (cf. triplet–triplet) time scales. To discriminate between these possibilities, we compare the nonlinear molecular absorption coefficients (i.e., combination of cross sections) obtained at two different repetition rates: f = 1 kHz (1 ms between pulses) and 76 MHz (13 ns between pulses). If there is a long-lived (13 ns < τ < 1 ms) intermediate state, then it will accumulate under the 76 MHz excitation but not upon 1 kHz excitation and therefore the observed nonlinear coefficients will be different. Alternatively, if the excited singlet (S_1, S_m, or S_n) works as an intermediate state, then the coefficients should be similar. By knowing the molecular cross sections and quantum yields contributing to the k_1 rate from the high repetition rate experiments (Table 2), we can substitute these parameters into the expressions for the k_1 rate but with the laser parameters corresponding to the low repetition rate conditions (i.e., with amplifier excitation), and we can compare the calculated values with those measured experimentally in Section 2.2.1. One can show (Supporting Information) that in the three-level system, i.e., in the DsRed2 case, with the possibility of saturation of the $m \rightarrow n$ transition and under spatially uniform illumination, as in the amplifier experiment

$$k_1^{(3)} = \frac{\sigma_2\phi_n f I_0}{8\sigma_{mn}}[X - 1 + e^{-X}], \quad \text{where } X = P/P_s \tag{20}$$

Substituting σ_{mn} and φ_n obtained for DsRed2 in the 76 MHz experiment and the laser parameters corresponding to the low repetition rate experiment into eq 20, we obtain $k_1^{(3)} = 1.4 \times 10^{-3}$ s^{-1}, which coincides with the measured value (Table 1).

For the four-level system with possible saturation, one obtains (Supporting Information)

$$k_1^{(4)} = \frac{\sigma_2\sigma_{nc} f}{32\sigma_{mn}^3\Delta\tau}\left[\frac{1}{2}X^3 - X^2 + X - Xe^{-X}\right], \quad \text{where } X = P/P_s \tag{21}$$

The rates estimated from eq 21 for mFruits also match well (within experimental errors) with those obtained using the amplifier system (see Table 1). These results suggest that the excited-state absorption proceeds through the singlet manifold in the RFPs under study (similar to that of EGFP[16,17]). Another important conclusion is that the rate of the process does not depend on the local environment (i.e., buffer vs *E. coli* cell).

3. DISCUSSION

Although the full MPB process comprises a complex chain of reactions, it appears that the rate of the first, $A \rightarrow B$, step, k_1, represents a good qualitative metric for the long-term kinetics. Under the experimental conditions of the amplifier setup, both k_1 and the inverse half-time of the full decay show the following sequence in the bleaching rates: mPlum > mCherry > mStrawberry ≈ DsRed2 (Supporting Information Figure 14). Therefore, understanding of the detailed elementary mechanisms of the $A \rightarrow B$ transformation is crucial for creating more photostable mutants.

dx.doi.org/10.1021/jp502477c | J. Phys. Chem. B 2014, 118, 9167–9179

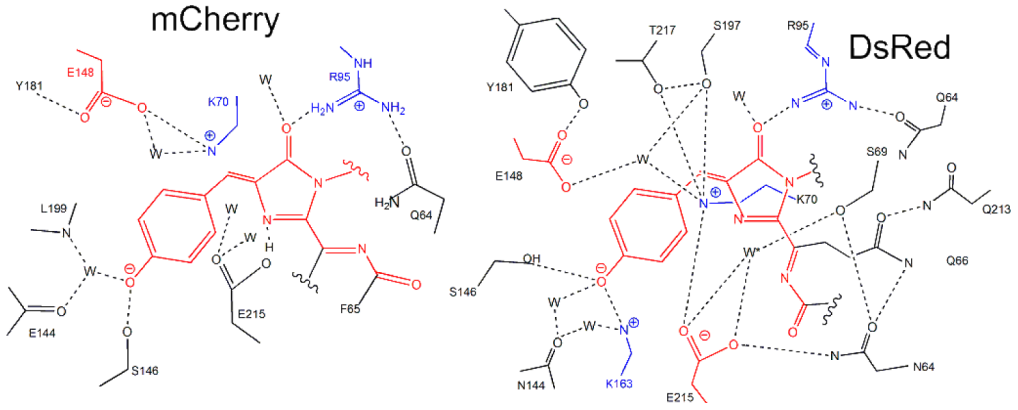

Figure 8. Schematic diagram of the mCherry (left) and DsRed (right) chromophore environments.[41,44] Hydrogen bonds are presented by dashed lines, charged groups are highlighted with color (blue, positive; red, negative), and water molecules are designated as W.

For DsRed2, the 2 + 1 phenomenological mechanism emerged from our analysis. Because the binding energy of the valence π electron in the anionic chromophore is quite low, VDE_0 = 3.27 eV,[23] the simultaneous absorption of two 790 nm photons ($2h\nu$ = 3.14 eV) excites a bound π^* state (m) slightly below the top of the chromophore potential well. The third photon absorption provides enough energy ($3h\nu$ = 4.71 eV) to remove the electron from the chromopohore valence state. In that higher-energy state (n), the electron becomes more delocalized, but it still remains close to the chromophore, bound by the net attractive Coulomb potential of the positive amino acid residues: K70, K83, R95, and K163 (see Section 2.4.2). The closest positive charge belongs to the protonated ε-amino group of K70, found just ∼3.7 Å away from the geometrical center of the chromophore (bridge carbon atom CB2), which contributes most to the local Coulomb potential. The $-NH_3^+$ ion of this residue presents a closed-shell core that can accept an electron to become the $-NH_3^\bullet$ radical.[43]

In the Kolbe decarboxylation mechanism, the first step consists of an electron transfer from the deprotonated glutamate group of a nearby acidic residue (probably E215 in the case of DsRed) to the chromophore.[20,21] This process is more probable for the neutral, not anionic, chromophore, because the former has larger electron affinity. Therefore, we can assume that the initial multiphoton-induced electron transfer to the nearby positive residue (e.g., K70) triggers this reaction by turning the chromophore into a neutral radical form. The next step is the Kolbe decarboxylation of the oxidized E215 residue

$$\text{Glu215}-CH_2-CH_2-CO_2^\bullet$$
$$\rightarrow CO_2 + \text{Glu215}-CH_2-CH_2^\bullet$$

Finally, the $-CH_2^\bullet$ radical, produced in this reaction, should recombine with either a hydrogen atom or accept an electron and proton. Because the hydrogen atom or proton can be transferred only on short distances, the hydrogen-donating group should be in close contact with the decarboxylated residue. In the DsRed2 protein, the E215 residue makes a close hydrogen-bonding contact with the protonated ε-amino group of K70 (Figure 8, right). As mentioned above, the $-NH_3^+$ group of K70 turns into the ammonium radial $-NH_3^\bullet$ after electron transfer from the chromophore. It is known that $-NH_3^\bullet$ in the ground state is metastable with respect to the $-NH_3^\bullet \rightarrow NH_2 + H^\bullet$ reaction.[43,45,46] Because of the close distance between K70 and E215, the released hydrogen may eventually recombine with the remaining $-CH_2^\bullet$ radical of E215.

Spectrally, the bleaching process is related to the chromophore isomerization, with the *trans* isomer showing much weaker fluorescence.[20] It is interesting to note that upon multiphoton excitation the anionic *trans* isomer is produced with the quantum yield of $\varphi_n = 8.8 \times 10^{-3}$, which exceeds the corresponding yield of one-photon *cis*–*trans* isomerization by 2 orders of magnitude ($\varphi_1 = 7.1 \times 10^{-5}$, ref 31), in agreement with previous qualitative observation.[20] Such acceleration of the process can be explained by the fact that the multiphoton-triggered decarboxylation leads to significant changes in the chromophore surrounding,[20] including the formation of extra free volume near the chromophore, rearrangement of hydrogen bonds, and redistribution of electrostatic potential.

In mFruits, in contrast to DsRed2, the E215 residue is protonated[41,42] and therefore cannot serve as an electron donor in Kolbe reaction. The closest deprotonated acidic residue to the chromophore is E148 (∼6.2 Å from the chromophore center) (Figure 8, left). The positively charged K70 residue is significantly displaced compared to its position in DsRed[40] and now makes a hydrogen-bonding contact with E148. If the multiphoton transformation is again coupled to Kolbe decarboxylation (of E148 now), we can assume that after the electron hopping from E148 to the chromophore and decarboxylation of the former, the hydrogen atom from the $-NH_3^\bullet$ radical of K70 can recombine with the $-CH_2^\bullet$ radical of E148. Our experimental results and quantum calculations suggest, however, that, in contrast to DsRed, the MPB reaction starts only if the electron is moved further from the closest surrounding of the chromophore (after four-photon photodetachment). It is not clear what causes this difference. We speculate that in mFruits, after its initial detachment, the electron probably returns to K70 to produce the $-NH_3^\bullet$ radical. The initial electron removal from the closest surrounding is probably needed because otherwise it can return to the chromophore faster than the electron transfer in the Kolbe reaction ($E148^- + Chro \rightarrow E148^\bullet + Chro^-$) takes place. This may imply that the Kolbe reaction occurs in mFruits slower than in DsRed2, probably because, among other reasons, of the longer distance from E148 to the chromophore in mFruits (∼6.2 Å) than from E215 to the chromophore in DsRed (∼4.9 Å). Similar to DsRed, the decarboxylation of E148 significantly changes the local surrounding (by creating larger free volume, rearranging hydrogen bonds, and changing

dx.doi.org/10.1021/jp502477c | J. Phys. Chem. B 2014, 118, 9167–9179

electrostatic potential), which can lead to fast chromophore isomerization.

It is interesting that the back ($A \leftarrow B$) reaction is activated even by five photons, as shown for mPlum. We may assume a similar, electron-transfer-mediated isomerization reaction for the anionic chromophore in the *trans* position. Because the chromophore geometry is different, other stepping-stone groups can come into play and therefore a fine balance of energetic and kinetic conditions can require more photons to promote the back reaction. The $B \rightarrow C$ step, corresponding to the multiphoton-activated protonation of the chromophore's phenoxy group and observed only in mFruits, may include a fast electron transfer to the remaining positively charged center, most probably R95, with subsequent hydrogen atom ejection from it, according to the reaction. The hydrogen atom may then bind to the phenolate oxygen of the chromophore radical and create a hydrogen-bonding contact with the remaining NH_2 group of R95 (cf. molecular structure of PAmCherry[32]). The close contact would allow excited-state proton transfer from the protonated chromophore (C-structure) to R95, thus explaining its red-shifted fluorescence (identical to that of the anionic B-structure).

4. CONCLUSIONS

On the long time-scale, the photobleaching process of RFPs comprises a chain of consecutive steps, with the first being a photoreversible step, $A \leftrightarrow B$, followed by irreversible transitions, $B \rightarrow C \rightarrow$ ..., to the nonfluorescent (upon 790 nm excitation) final products. All individual phototransformation steps, including the reverse $A \leftarrow B$ reaction, are induced by high-order (3−5) photon absorption. High nonlinearities of these reactions can find use in the recently proposed methods of deep imaging based on multiphoton activation.[7,8]

In DsRed2, the intermediate form B can be spectrally assigned to the anionic *trans* isomer of the chromophore. In mFruits, there are two intermediate forms with the same fluorescence but different absorption spectra, which we assign to the *trans* chromophore deprotonated (B) and protonated (C) at the phenoxy group, respectively.

Our results suggest that in the first elementary step of the $A \rightarrow B$ transformation the initial instantaneous two-photon absorption step is followed by a sequential absorption of additional one (in DsRed2) or two (mFruits) photons. The comparison of the rate constants measured with different repetition rates (1 kHz vs 76 MHz) indicates that the additional photons are absorbed from the same femtosecond pulse and therefore correspond to singlet−singlet transitions without involvement of longer-living (e.g., triplet) states. Considering the order of the process (number of photons involved) in combination with the reaction energetics (calculated electron detachment energies for the chromophore in protein environment), it appears that in DsRed2 the reaction proceeds from a bound state, where the electron, originating from the HOMO of the chromophore, is still bound to its closest environmental shell. In mFruits, the first step of the reaction corresponds to the electron detachment from the nearest surrounding of the chromophore. The dependence of the rates on pulse duration and energetic considerations lead us to the conclusion that little or no energy relaxation takes place between sequential steps of multiphoton absorption during 100−200 fs. Careful measurements of the power dependences of the rates supported by the kinetics simulations with the rate equations of the three- and four-level systems demonstrate that the empirical noninteger power exponent can be better explained in terms of saturation of one of the stepwise one-photon transitions than it can as a result of combination of parallel process of different order (e.g., three- and four-photon excitation). The saturation is slight in DsRed2, but it is moderately strong in mFruits. We also show that the bleaching rates are very similar in buffer solution and an *E. coli* cell environment, suggesting purely intramolecular mechanisms of the $A \rightarrow B$ step.

Some particular details of the ultrafast photochemistry of this step can further be suggested. In DsRed2, the third photon absorption most probably corresponds to the charge-transfer transition from an excited π^* orbital of the anionic chromophore to a nearby positive amino acid residue (K70). The transient radical state of the chromophore tends to accept an electron, most probably from the deprotonated E215 amino acid residue, thus promoting the first step of the recently established decarboxylation reaction[20] that eventually leads to the *cis*−*trans* isomerization of the chromophore. This latter process is strongly enhanced in the case of multiphoton excitation, compared to linear excitation of the S_1 level, which can be explained by the creation of more space near the chromophore, rearrangement of the local hydrogen-bonding network, and redistribution of local electrostatic potential after decarboxylation reaction. In mFruits, lacking a negative charge at the E215, the Kolbe decarboxylation of another deprotonated residue, E148, may trigger the *cis*−*trans* isomerization of the chromophore, similar to that in DsRed. In contrast to DsRed2, the first step of the multiphoton process probably involves the detachment of an electron from the local electrostatic potential, created mostly by two positive residues, K70 and R95.

The mechanism described here points to possibilities for improving the photostability of red FPs by manipulating, through mutagenesis, the key amino acids participating in multiphoton bleaching. In addition to K70, K95, E148, and E215, there are other charged amino acids, including D59, D81, K84, K83, and K163 (the last two are charged in DsRed2 but are substituted to neutral residues in mFruits), whose position displacement or substitution may alter the electrostatic potential near the chromophore and therefore result in a change of the energetics of the underlying electron-transfer reactions.

■ ASSOCIATED CONTENT

Supporting Information

Experimental details and methods of the photobleaching measurements in *E. coli* colonies, in purified buffer solutions, and in HEK cells; details on quantum calculation of electrostatic potential energy created by protein environment at the chromophore atoms; derivation of eqs 14−21; fluorescence spectrum changes after one-photon irradiation of mFruits in buffer solution; spectral decomposition of the fluorescence spectra of DsRed2 and mCherry at intermediate stages of bleaching; absorption spectrum changes during multiphoton bleaching of mPlum in buffer solution; intensity dependence of initial fluorescence signal obtained at 76 MHz repetition rate in *E. coli* colonies and at 1 kHz repetition rate in buffer solution; photobleaching decay kinetics of DsRed2 and mPlum; decay of the fluorescence signal of mCherry expressed in *E. coli*; and multiphoton decay kinetics of RFP in buffer solution under continuous irradiation with a Ti:Sa amplifier. This material is available free of charge via the Internet at http://pubs.acs.org.

dx.doi.org/10.1021/jp502477c | J. Phys. Chem. B 2014, 118, 9167−9179

AUTHOR INFORMATION

Corresponding Author

*E-mail: drobizhev@physics.montana.edu.

Notes

The authors declare no competing financial interest.

ACKNOWLEDGMENTS

This work was supported by NIH grants R01 GM 098083 and 1 R01 NS083875-01. We thank Pat Callis and Anton Vorontsov for very stimulating discussions. I.T. and J.C. thank the staff and administration of the Advanced Biomedical Computing Center for their support of this project. This project was funded in whole or in part with federal funds from the National Cancer Institute, National Institutes of Health, under contract no. HHSN261200800001E. The content of this publication does not necessarily reflect the views or policies of the Department of Health and Human Services, nor does mention of trade names, commercial products, or organization imply endorsement by the U.S. government.

REFERENCES

(1) Tsien, R. Y. The Green Fluorescent Protein. *Annu. Rev. Biochem.* **1998**, *67*, 509−544.

(2) Frommer, W. B.; Davidson, M. W.; Campbell, R. E. Genetically Encoded Biosensors Based on Engineered Fluorescent Proteins. *Chem. Soc. Rev.* **2009**, *38*, 2833−2841.

(3) Barnett, L.; Platisa, J.; Popovic, M.; Pieribone, V. A.; Hughes, T. A Fluorescent, Genetically-Encoded Voltage Probe Capable of Resolving Action Potentials. *PLoS One* **2012**, *7*, e43454.

(4) Akerboom, J.; Calderon, N. C.; Tian, L.; Wabnig, S.; Prigge, M.; Tolo, J.; Gordus, A.; Orger, M. B.; Severi, K. E.; Macklin, J. J.; et al. Genetically Encoded Calcium Indicators for Multi-Color Neural Activity Imaging and Combination with Optogenetics. *Front. Mol. Neurosci.* **2013**, *6*, 2.

(5) Denk, W.; Strickler, J. H.; Webb, W. W. 2-Photon Laser Scanning Fluorescence Microscopy. *Science* **1990**, *248*, 73−76.

(6) Diaspro, A.; Chirico, G.; Collini, M. Two-photon fluorescence excitation and related techniques in biological microscopy. *Q. Rev. Biophys.* **2005**, *38*, 97−166.

(7) Zhu, X.; Kao, Y.-T.; Min, W. Molecular-Switch-Mediated Multiphoton Fluorescence Microscopy with High-Order Nonlinearity. *J. Phys. Chem. Lett.* **2012**, *3*, 2082−2086.

(8) Yao, J. J.; Wang, L. D.; Li, C. Y.; Zhang, C.; Wang, L. H. V. Photoimprint Photoacoustic Microscopy for Three-Dimensional Label-Free Subdiffraction Imaging. *Phys. Rev. Lett.* **2014**, *112*, 014302.

(9) Theer, P.; Denk, W. On the Fundamental Imaging-Depth Limit in Two-Photon Microscopy. *J. Opt. Soc. Am. A* **2006**, *23*, 3139−3149.

(10) Bal, U.; Andresen, V.; Baggett, B.; Utzinger, U. Intravital Confocal and Two-Photon Imaging of Dual-Color Cells and Extracellular Matrix Mimics. *Microsc. Microanal.* **2013**, *19*, 201−212.

(11) Patterson, G. H.; Piston, D. W. Photobleaching in Two-Photon Excitation Microscopy. *Biophys. J.* **2000**, *78*, 2159−2162.

(12) Hess, S. T.; Sheets, E. D.; Wagenknecht-Wiesner, A.; Heikal, A. A. Quantitative Analysis of the Fluorescence Properties of Intrinsically Fluorescent Proteins in Living Cells. *Biophys. J.* **2003**, *85*, 2566−2580.

(13) Robinson, L. C.; Marchant, J. S. Improved "Optical Highlighter" Probes Derived from Discosoma Red Fluorescent Protein. *Biophys. J.* **2005**, *88*, 1444−1457.

(14) Drummond, D. R.; Carter, N.; Cross, R. A. Multiphoton versus Confocal High Resolution z-Sectioning of Enhanced Green Fluorescent Microtubules: Increased Multiphoton Photobleaching within the Focal Plane Can Be Compensated Using a Pockels Cell and Dual Widefield Detectors. *J. Microsc.* **2002**, *206*, 161−169.

(15) Herz, J.; Siffrin, V.; Hauser, A. E.; Brandt, A. U.; Leuenberger, T.; Radbruch, H.; Zipp, F.; Niesner, R. A. Expanding Two-Photon Intravital Microscopy to the Infrared by Means of Optical Parametric Oscillator. *Biophys. J.* **2010**, *98*, 715−723.

(16) Kalies, S.; Kuetemeyer, K.; Heisterkamp, A. Mechanisms of High-Order Photobleaching and Its Relationship to Intracellular Ablation. *Biomed. Opt. Express* **2011**, *2*, 805−816.

(17) Ji, N.; Magee, J. C.; Betzig, E. High-Speed, Low-Photodamage Nonlinear Imaging Using Passive Pulse Splitters. *Nat. Methods* **2008**, *5*, 197−202.

(18) Donnert, G.; Eggeling, C.; Hell, S. W. Major Signal Increase in Fluorescence Microscopy through Dark-State Relaxation. *Nat. Methods* **2007**, *4*, 81−86.

(19) Field, J. J.; Carriles, R.; Sheetz, K. E.; Chandler, E. V.; Hoover, E. E.; Tillo, S. E.; Hughes, T. E.; Sylvester, A. W.; Kleinfeld, D.; Squier, J. A. Optimizing the Fluorescent Yield in Two-Photon Laser Scanning Microscopy with Dispersion Compensation. *Opt. Express* **2010**, *18*, 13661−13672.

(20) Habuchi, S.; Cotlet, M.; Gensch, T.; Bednarz, T.; Haber-Pohlmeier, S.; Rozenski, J.; Dirix, G.; Michiels, J.; Vanderleyden, J.; Heberle, J.; et al. Evidence for the Isomerization and Decarboxylation in the Photoconversion of the Red Fluorescent Protein DsRed. *J. Am. Chem. Soc.* **2005**, *127*, 8977−8984.

(21) Van Thor, J. J.; Gensch, T.; Hellingwerf, K. J.; Johnson, L. N. Phototransformation of Green Fluorescent Protein with UV and Visible Light Leads to Decarboxylation of Glutamate 222. *Nat. Struct. Biol.* **2002**, *9*, 37−41.

(22) Vegh, R. B.; Bravaya, K. B.; Bloch, D. A.; Bommarius, A. S.; Tolbert, L. M.; Verkhovsky, M.; Krylov, A. I.; Solntsev, K. M. Chromophore Photoreduction in Red Fluorescent Proteins Is Responsible for Bleaching and Phototoxicity. *J. Phys. Chem. B* **2014**, *118*, 4527−4534.

(23) Ghosh, D.; Acharya, A.; Tiwari, S. C.; Krylov, A. I. Toward Understanding the Redox Properties of Model Chromophores from the Green Fluorescent Protein Family: An Interplay between Conjugation, Resonance Stabilization, and Solvent Effects. *J. Phys. Chem. B* **2012**, *116*, 12398−12405.

(24) Yanushevich, Y. G.; Staroverov, D. B.; Savitsky, A. P.; Fradkov, A. F.; Gurskaya, N. G.; Bulina, M. E.; Lukyanov, K. A.; Lukyanov, S. A. A Strategy for the Generation of Non-aggregating Mutants of Anthozoa Fluorescent Proteins. *FEBS Lett.* **2002**, *511*, 11−14.

(25) Shaner, N. C.; Campbell, R. E.; Steinbach, P. A.; Giepmans, B. N. G.; Palmer, A. E.; Tsien, R. Y. Improved Monomeric Red, Orange and Yellow Fluorescent Proteins Derived from *Discosoma* sp. Red Fluorescent Protein. *Nat. Biotechnol.* **2004**, *22*, 1567−1572.

(26) Wang, L.; Jackson, W. C.; Steinbach, P. A.; Tsien, R. Y. Evolution of New Nonantibody Proteins via Iterative Somatic Hypermutation. *Proc. Natl. Acad. Sci. U.S.A.* **2004**, *101*, 16745−16749.

(27) Kremers, G.-J.; Hazelwood, K. L.; Murphy, C. S.; Davidson, M. W.; Piston, D. W. Photoconversion in Orange and Red Fluorescent Proteins. *Nat. Methods* **2009**, *6*, 355−358.

(28) Nienhaus, K.; Nar, H.; Heilker, R.; Wiedenmann, J.; Nienhaus, G. U. Trans−Cis Isomerization Is Responsible for the Red-Shifted Fluorescence in Variants of the Red Fluorescent Protein eqFP611. *J. Am. Chem. Soc.* **2008**, *130*, 12578−12579.

(29) Hendrix, J.; Flors, C.; Dedecker, P.; Hofkens, J.; Engelborghs, Y. Dark States in Monomeric Red Fluorescent Proteins Studied by Fluorescence Correlation and Single Molecule Spectroscopy. *Biophys. J.* **2008**, *94*, 4103−4113.

(30) Dean, K. M.; Lubbeck, J. L.; Binder, J. K.; Schwall, L. R.; Jimenez, R.; Palmer, A. E. Analysis of Red-Fluorescent Proteins Provides Insight into Dark-State Conversion and Photodegradation. *Biophys. J.* **2011**, *101*, 961−969.

(31) Drobizhev, M.; Hughes, T. E.; Stepanenko, Y.; Wnuk, P.; O'Donnell, K.; Scott, J. N.; Callis, P. R.; Mikhaylov, A.; Dokken, L.; Rebane, A. Primary Role of the Chromophore Bond Length Alternation in Reversible Photoconversion of Red Fluorescence Proteins. *Sci. Rep.* **2012**, *2*, 688.

(32) Subach, F. V.; Malashkevich, V. N.; Zencheck, W. D.; Xiao, H.; Filonov, G. S.; Almo, S. C.; Verkhusha, V. V. Photoactivation Mechanism of PAmCherry Based on Crystal Structures of the Protein

in the Dark and Fluorescent States. *Proc. Natl. Acad. Sci. U.S.A.* **2009**, *106*, 21097−21102.
(33) Kogure, T.; Karasawa, S.; Araki, T.; Saito, K.; Kinjo, M.; Miyawaki, A. A Fluorescent Variant of a Protein from the Stony Coral Montipora Facilitates Dual-Color Single-Laser Fluorescence Cross-Correlation Spectroscopy. *Nat. Biotechnol.* **2006**, *24*, 577−581.
(34) Piatkevich, K. D.; Malashkevich, V. N.; Almo, S. C.; Verkhusha, V. V. Engineering ESPT Pathways Based on Structural Analysis of LSSmKate Red Fluorescent Proteins with Large Stokes Shift. *J. Am. Chem. Soc.* **2010**, *132*, 10762−10770.
(35) Drobizhev, M.; Makarov, N. S.; Tillo, S.; Hughes, T. E.; Rebane, A. Two-Photon Absorption Properties of Fluorescent Proteins. *Nat. Methods* **2011**, *8*, 393−399.
(36) Piatkevich, K. D.; Hulit, J.; Subach, O. M.; Wu, B.; Abdulla, A.; Segall, J. E.; Verkhusha, V. V. Monomeric Red Fluorescent Proteins with a Large Stokes Shift. *Proc. Natl. Acad. Sci. U.S.A.* **2010**, *107*, 5369−5374.
(37) Eggeling, C.; Volkmer, A.; Seidel, C. A. M. Molecular Photobleaching Kinetics of Rhodamine 6G by One- and Two-Photon Induced Confocal Fluorescence Microscopy. *ChemPhysChem* **2005**, *6*, 791−804.
(38) Ambartsumyan, R. V.; Apatin, A. M.; Letokhov, V. S.; Makarov, A. A.; Mishin, V. I.; Puretskii, A. A.; Furzikov, N. P. Selective Two-Step Ionization of Rubidium by Laser Radiation. *J. Exp. Theor. Phys.* **1976**, *43*, 866−872.
(39) Goodman, L.; Philis, J. Multiphoton Absorption Spectroscopy. In *Applied Laser Spectroscopy: Techniques, Instrumentation, and Applications*; Andrews, D. L., Ed.; VCH Publishers: New York, 1992; Chapter 8, pp 319−364.
(40) Topol, I.; Collins, J.; Savitsky, A.; Nemukhin, A. Computational Strategy for Tuning Spectral Properties of Red Fluorescent Proteins. *Biophys. Chem.* **2011**, *158*, 91−95.
(41) Shu, X.; Shaner, N. C.; Yarbrough, C. A.; Tsien, R. Y. Novel Chromophores and Buried Charges Control Color in mFruits. *Biochem.* **2006**, *45*, 9639−9647.
(42) Shu, X.; Wang, L.; Colip, L.; Kalio, K.; Remington, S. J. Unique Interactions between the Chromophore and Glutamate 16 Lead to Far-Red Emission in a Red Fluorescent Protein. *Protein Sci.* **2009**, *18*, 460−466.
(43) Herzberg, G. Rydberg Molecules. *Annu. Rev. Phys. Chem.* **1987**, *38*, 27−56.
(44) Remington, S. J.; Wachter, R. M.; Yarbrough, D. K.; Branchaud, B.; Anderson, D. C.; Kallio, K.; Lukyanov, K. A. zFP538, a Yellow-Fluorescent Protein from Zoanthus, Contains a Novel Three-Ring Chromophore. *Biochemistry* **2005**, *44*, 202−212.
(45) Havriliak, S.; King, H. F. Rydberg Radicals 0.1. Frozen-Core Model for Rydberg Levels of the Ammonium Radical. *J. Am. Chem. Soc.* **1983**, *105*, 4−12.
(46) Nonose, S.; Taguchi, T.; Chen, F.; Iwata, S.; Fuke, K. Electronic Spectra and Structures of Solvated NH_4 Radicals, $NH_4(NH_3)_n$ (n = 1−8). *J. Phys. Chem. A* **2002**, *106*, 5242−5248.